

# The Application of Grain Boundary Engineering to a Nickel Base Superalloy for 973 K (700 °C) USC Power Plants

YAN CHONG, ZHENG DONG LIU, ANDY GODFREY, WEI LIU, and YUQING WENG

The microstructure of a Ni-base superalloy Inconel740H designed for the ultra-supercritical coal-fired power plants has been enhanced *via* grain boundary engineering. Single-step thermo-mechanical processing treatments were carried out to optimize the grain boundary character distribution (GBCD) and assessed based on the fraction of low- $\Sigma$  ( $\Sigma \leq 29$ ) coincidence site lattice (CSL) boundaries,  $f_{\text{CSL}}$ , as well as on the interrupted high-angle grain boundary (HAGB) network. Solution-annealed samples were compressed by 3, 6, 10, and 15 pct at room temperature followed by annealing at 1373 K (1100 °C) for between 5 and 40 minutes. For samples deformed to strains of values of less than 10 pct, deformation-induced grain boundary migration occurs and high values of  $f_{\text{CSL}}$ , with large cluster sizes, are obtained. For samples deformed to strains larger than 10 pct, static recrystallization dominates, resulting in decreased value of  $f_{\text{CSL}}$ . The highest  $f_{\text{CSL}}$  value ( $\approx 80$  pct) was obtained in the sample annealed at 1373 K (1100 °C) for 20 minutes after 6 pct cold deformation, in which the HAGB network was substantially interrupted. The triple junction distributions of samples before and after GBE were also studied. The introduction of large amounts of CSLBs after thermomechanical-processing treatment increased both fractions of  $J_2$  and  $J_3$  type junctions (triple junctions containing 2 or 3 CSL boundaries), therefore leading to a significant increase in the resistant triple junction fraction, defined as  $f_{J_2}/(1 - f_{J_3})$ . In addition, the thermal stability of the GBCD-optimized microstructure was confirmed to be stable at 1023 K (750 °C) for 500 hours without significant decrease in  $f_{\text{CSL}}$ .

DOI: 10.1007/s40553-014-0009-6

© The Minerals, Metals & Materials Society and ASM International 2014

## I. INTRODUCTION

INCONEL740H is a newly developed Ni-base superalloy used for the main steam pipes and superheater tubes of 973 K (700 °C) ultra-supercritical coal-fired power plants. The alloy requirements are a high creep rupture strength (at least 100 MPa in  $10^5$  hours) and high corrosion resistance (less than 2 mm loss in cross section in  $2 \times 10^5$  hours) at the operating temperature range of 973 K to 1023 K (700 °C to 750 °C). The nominal composition of Inconel740H is 25Cr, 20Co, 0.5Mo, 1.5Nb, 1.4Ti, 1.4Al, 0.3Mn, 0.03Fe, 0.03C, and Ni balance (wt pct). The alloy is solution strengthened by its content of Co. By virtue of its high Cr content, the alloy exhibits excellent resistance to oxidation, carburization, and sulfidation at high temperatures. After a standard heat treatment (solution annealing plus aging), the microstructure of Inconel740H consists of a coarse  $\gamma$  matrix with finely dispersed  $\gamma'$  inside the  $\gamma$  matrix and continuous  $M_{23}C_6$  carbides at the grain boundaries.<sup>[1-4]</sup> In creep rupture samples, it is found that cracks initiate at grain boundaries and propagate through the network of high-angle grain boundaries.<sup>[5,6]</sup> Therefore, it is

expected that enhancements to the grain boundary characteristics in Inconel740H may help to extend the service lifetime and thus maintain system stability.

Grain boundary engineering, first proposed by Watanabe<sup>[7]</sup> in 1984, has found extensive applications in low-to-medium stacking fault energy materials such as OFE copper,<sup>[8]</sup> nickel base superalloys,<sup>[9-11]</sup> and austenite steels.<sup>[12]</sup> The central premise of GBE is that specific thermomechanical-processing treatments, mainly on face-centered cubic materials that readily form annealing twins, can be utilized to improve resistance to various intergranular degradations such as intergranular stress corrosion cracking (IGSCC),<sup>[9,13,14]</sup> creep,<sup>[15,16]</sup> and embrittlement<sup>[17]</sup> by promoting a high proportion of low- $\Sigma$  ( $\Sigma \leq 29$ ) coincidence site lattice (CSL) boundaries. CSL boundaries are characterized by specific values of misorientation which allow atoms from neighboring lattices notionally to coincide.<sup>[18,19]</sup> The  $\Sigma$  value is defined as the reciprocal fraction of coincidence sites. The low distortion of bonding atoms and relatively small free volume at CSL boundaries are presumed to result in low grain boundary energies.

Two evaluation criteria have been proposed to evaluate the effectiveness of GBE; one is the increase of CSL boundary fraction at the expense of HAGBs. Substantial improvements in properties such as creep<sup>[15,16]</sup> and IGSCC<sup>[9,13,14]</sup> have been found to correlate with increases in CSL boundary fraction in grain boundary-engineered materials. However, the CSL boundary fraction alone cannot describe the grain boundary network topology, which is of prime

YAN CHONG, Ph.D. Candidate, ANDY GODFREY, Professor, and WEI LIU, Professor, are with the School of Materials Science and Engineering, Tsinghua University, Beijing, P. R. China. Contact e-mail: chongyan871210@sina.com ZHENG DONG LIU, Professor, and YUQING WENG, Professor, are with the China Iron and Steel Research Institute, Beijing, P. R. China.

Manuscript submitted November 6, 2013.

Article published online February 15, 2014

importance in mitigating intergranular failure. In the previous investigations, two methods have been proposed to quantify grain boundary connectivity.<sup>[20]</sup> The first method is based on the statistics of triple junction types, in which the triple junctions are classified according to the number of CSL boundaries they contain thus providing an indicator of resistance to failure. It is believed that triple junctions containing two CSL boundaries can arrest the propagation of crack and therefore an increased fraction of such triple junctions is highly desirable. Kumar *et al.*<sup>[21]</sup> proposed, on the basis of percolation theory, that a resistant triple junction fraction of less than 65 pct (excluding inactive triple junctions which contains three CSL boundaries) can pose no barrier to crack for the percolation of crack percolation. Accordingly, the following inequality for resistant triple junctions should be satisfied in order to arrest crack propagation,

$$\frac{f_{2\text{CSL}}}{(1 - f_{3\text{CSL}})} \geq 0.35$$

in which,  $f_{2\text{CSL}}$  refers to the fraction of triple junctions containing two CSL boundaries and  $f_{3\text{CSL}}$  is the fraction of triple junctions with three CSL boundaries. It should be noted that cracks are assumed never to reach 3-CSL boundary junctions; therefore 3-CSL boundary junctions do not play a role in crack arrest and are excluded from the percolation analysis. The second criterion for quantifying grain boundary connectivity is *via* cluster mass analysis.<sup>[22]</sup> A ‘cluster’ is defined as an interconnected grain boundary network of the same type, and the mass of a cluster is defined as the total length of boundaries contained in the cluster. Another length of interest is the maximum linear dimension of a cluster, as this may govern the length of intergranular cracks.<sup>[23]</sup> According to the research of Schuh *et al.*,<sup>[24]</sup> the fragmentation of HAGB network by grain boundary engineering is found to involve at least an order-of-magnitude decrease in the HAGB cluster mass. Moreover, Tsurekawa *et al.*<sup>[23]</sup> found that the maximum length of HAGB clusters decreased dramatically with increasing frequency of CSL boundary fractions especially at the percolation threshold of approximately  $70 \pm 5$  pct CSL boundary fraction, or approximately 35 pct of resistant triple junctions.

## II. MATERIALS AND METHODS

The as-received Inconel740H alloy, with chemical composition in Table I, was solution annealed (SA) at 1423 K (1150 °C) for 30 minutes and quenched in water. Cylindrical samples with diameter of 8 mm and height of 12 mm were machined from the solution-annealed alloy. Single-step thermomechanical treatment

was carried out at room temperature. The samples were compressed to four different levels of strain (3, 6, 10, and 15 pct) along the length of each cylinder, followed by annealing at 1373 K (1100 °C) for four different durations (5, 10, 20, and 40 minutes). It should be noted that all the strains referred to in this study are engineering strains. After annealing, the samples were water quenched.

Samples after the thermomechanical-processing treatments were cut parallel to the compression axis at the geometric center. The cut surfaces were mechanically polished with SiC abrasive paper down to 1000 grit followed by sequential polishing to 0.5  $\mu\text{m}$  diamond paste. A final electro-polishing was carried out in a solution containing 10 pct  $\text{HClO}_4$  + 90 pct  $\text{CH}_3\text{CH}_2\text{OH}$  using 15 V direct current. Electron backscattered diffraction (EBSD) was used to determine the grain boundary misorientations using Oxford system attached to a field-emission gun scanning electron microscope (Tescan LYRA3). In this work, grain boundaries with  $\Sigma \leq 29$  were regarded as low- $\Sigma$  CSL boundaries. For EBSD measurements, SEM was operated at 20 kV and automated scans were performed over areas of  $2000 \times 2000 \mu\text{m}^2$ , with a step size of 5  $\mu\text{m}$ . Two or three areas near the center of the cut surfaces were examined of each sample after thermomechanical-processing treatment. At least 500 grains were covered in the EBSD maps for each sample. Brandon criterion was used to establish the CSL fraction with the maximum allowable misorientation ( $\Delta\theta$ ) deviation from the exact CSL given by  $\Delta\theta = \Delta\theta_m \Sigma^{-1/2}$ , in which  $\Delta\theta_m$  is the maximum misorientation angle for a low angle grain boundary (typically 15 deg). The minimum misorientation to determine a grain boundary was 2 deg. The GBCD data are reported here as length fractions as calculated by the EBSD software.

## III. RESULTS AND DISCUSSION

### A. The Comparison Before and After Grain Boundary Engineering

The length fractions of  $\Sigma 3$ ,  $\Sigma 9$ ,  $\Sigma 27$ , and total CSL boundary of SA and grain boundary-engineered samples are shown in Tables II and III. The microstructures of the SA and one example of the grain boundary-engineered samples are shown in Figure 1. In the grain boundary-engineered sample, 3 pct strain and 20 minutes annealing at 1373 K (1100 °C) were applied. In Figures 1(a) through (c), the microstructures of the SA sample are shown, with Figure 1(a) showing both CSL boundaries and HAGBs, Figure 1(b) showing CSL boundaries only, while Figure 1(c) showing HAGBs only. The microstructures of the grain boundary-engineered sample are shown in Figures 1(d) through (f),

Table I. Chemical Composition of Inconel740H (wt pct)

Element	Cr	Co	Mo	Ti	Al	Nb	Mn	Si	Fe	C	S	Ni
Wt pct	25.48	20.17	0.50	1.38	1.47	1.48	0.34	0.049	0.032	0.023	0.001	Bal.

respectively. The length fraction of CSL boundary ( $f_{\text{CSL}}$ ) increased from 61 pct in the SA sample to 74 pct in the grain boundary-engineered sample, confirming the applicability of grain boundary engineering in Inconel740H. In the SA sample, the fractions of  $\Sigma 9$  and  $\Sigma 27$  boundaries are negligible, while a significant increase in both the  $\Sigma 9$  and  $\Sigma 27$  boundary fractions is found after grain boundary engineering, indicating the occurrence of multi-twinning during thermomechanical processing. The result is consistent with other investigations of grain boundary engineering in low-to-medium stack fault energy alloys.<sup>[12,23,25–27]</sup> In the SA sample, CSL boundaries (mostly coherent twin boundaries) typically cut straight through individual grains, leaving flat, isolated interfaces. In contrast, CSL boundaries in the grain boundary-engineered sample are curved and intersect with each other, as is usually seen in grain boundary-engineered materials. It is believed, however, that an increase of CSL boundary fraction alone cannot necessarily guarantee the effectiveness of grain boundary engineering. More important is the effect of grain boundary engineering on the break-up in connectivity of the HAGB network. It can be seen from Figures 1(c) and (f) that in the SA sample, the HAGBs are well connected and provide potential propagation path for creep cracks. However, in the grain boundary-engineered sample, HAGB connectivity is interrupted by the incorporation of CSL boundaries into the HAGB network. In addition, the size of the area bounded by HAGBs, which is defined as cluster (discussed in detail in the following section), is much larger in the grain boundary-engineered sample compared to the SA sample. Several clusters with size larger than 500  $\mu\text{m}$  are seen in Figure 1(f), while the cluster sizes in Figure 1(c) are all well below 200  $\mu\text{m}$ .

### B. The Evolution of $f_{\text{CSL}}$ with Strain and Annealing Time

The evolution of  $f_{\text{CSL}}$  (length fraction) with strain and annealing time is shown in Figure 2. It is found that  $f_{\text{CSL}}$  is influenced by both strain and annealing time. In samples deformed to strains of 3 and 6 pct strains, the

**Table II. Fractions of CSL Boundaries in Solution-Annealed Sample of Inconel740H**

Type	$\Sigma 3$	$\Sigma 9$	$\Sigma 27$
Fraction/pct	59.3	1.36	0.17

increase of  $f_{\text{CSL}}$  is obvious. For both strains,  $f_{\text{CSL}}$  increased with annealing time until reaching a peak at 20 minutes and remained stable afterward. It is noticed from Table III that the fractions of  $\Sigma 9$  and  $\Sigma 27$  boundaries also increased in the first 20 minutes, indicating the process of multi-twinning. In contrast, in samples deformed to strains larger than 10 pct, the increases of  $f_{\text{CSL}}$  were minor, with  $f_{\text{CSL}}$  actually decreasing in the samples with 15 pct strain. Therefore, for successfully applying grain boundary engineering in Inconel740H, the strain should be kept less than 6 pct and the annealing duration at 1373 K (1100 °C) should be more than 20 minutes.

### C. The Connectivity of HAGB Network

The scalar quantity of  $f_{\text{CSL}}$  cannot describe directly the grain boundary network topology, which is critical in mitigating intergranular failure. The increase of  $f_{\text{CSL}}$  cannot guarantee either the effectiveness of grain boundary engineering. As mentioned earlier, two commonly used methods to evaluate the connectivity of HAGB networks are by either triple junction analysis or cluster analysis. They are discussed in following sections.

#### 1. Triple junction analysis

In this analysis, we focus on the character of triple junctions, which are assumed to act as either a barrier or passage for crack propagations, depending on the type of grain boundaries at each junction. The triple junctions are classified according to the numbers of CSL boundaries they contain in a 2D section as ( $J_0$ ,  $J_1$ ,  $J_2$ , and  $J_3$ ). For example, two CSL boundaries are connected in  $J_2$  junctions, while none are connected in  $J_0$  junctions. The premise of such an analysis is that the CSL boundaries are intrinsically stable and the possibility of creep cracks propagating through CSL boundaries is much smaller compared with HAGBs, thus they can be considered as ‘safe’ during creep. Following this premise, a crack can easily propagate through  $J_0$  junctions, will be diverted at  $J_1$  junctions, stopped at  $J_2$  junctions, and can never reach  $J_3$  junctions. Hence it is desired to achieve a high fraction of  $J_2$  junctions after grain boundary engineering so as to arrest creep cracks. Note that in this study, only a two-dimensional triple junction distribution investigation was made for simplicity. Triple junction character distributions for SA and grain boundary-engineered samples are presented in Figure 3. In this case, the grain boundary-engineered

**Table III. Fractions of CSL Boundaries After Thermomechanical Processing of Inconel740H**

Length Fraction/pct	3 pct				6 pct				10 pct				15 pct			
	$\Sigma$	$\Sigma 3$	$\Sigma 9$	$\Sigma 27$	$\Sigma$	$\Sigma 3$	$\Sigma 9$	$\Sigma 27$	$\Sigma$	$\Sigma 3$	$\Sigma 9$	$\Sigma 27$	$\Sigma$	$\Sigma 3$	$\Sigma 9$	$\Sigma 27$
5 min	65.7	58.8	4.93	1.93	70.1	62.5	5.63	1.97	64.5	55.5	5.91	3.11	55.7	48.8	4.38	2.52
10 min	66.7	58.8	5.28	2.58	74.4	65.0	5.83	3.53	62.6	54.0	5.79	2.79	56.6	50.0	4.12	2.48
20 min	74.3	64.4	5.83	4.04	79.3	69.2	6.32	3.75	65.3	57.3	5.80	2.21	58.0	50.3	5.53	2.21
40 min	73.5	63.5	6.08	3.93	78.4	68.3	6.18	3.92	62.8	55.5	4.73	2.53	57.2	50.8	4.14	2.26



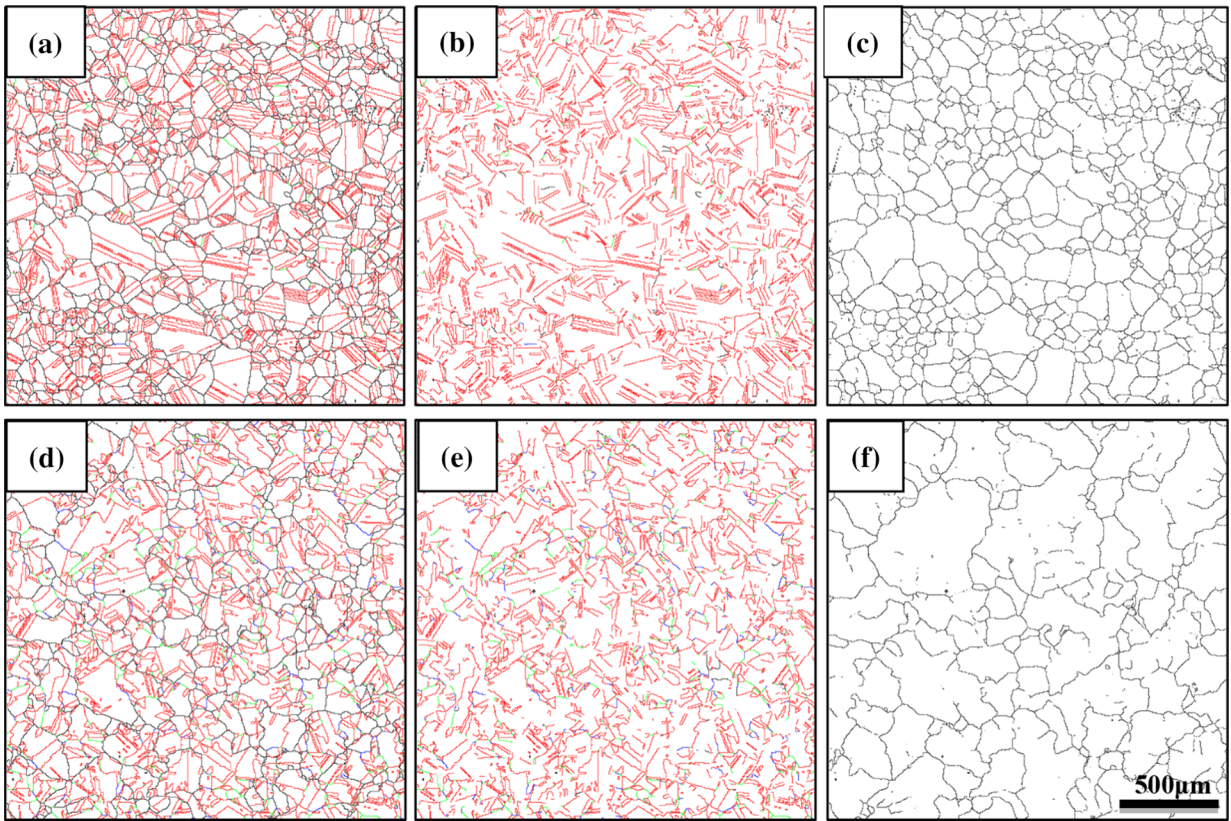


Fig. 1—GBCD before (a, b, c) and after (d, e, f) grain boundary engineering. a, d HAGBs and CSLBs. b, e Only CSLBs. c, f Only HAGBs (color code:  $\Sigma$ 3-red;  $\Sigma$ 9-green;  $\Sigma$ 27-blue; and HAGB-black) (Color figure online).

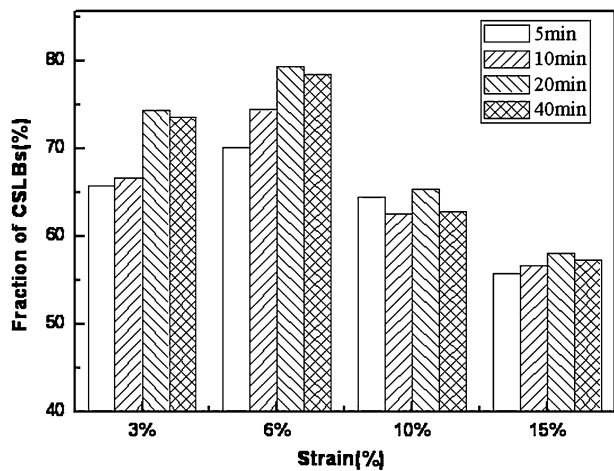


Fig. 2—The effect of thermomechanical-processing treatment parameters (strain and annealing time) on the total fraction of CSLB.

sample was deformed by 6 pct strain and annealed at 1373 K (1100 °C) for 20 minutes (optimal condition). At least 300 triple junctions were counted in each sample for statistical confidence. As seen in Figure 3, the fraction of  $J_2$  junctions increased from 1.8 to 12.6 pct and the fraction of  $J_3$  junctions increased from 1.6 to 20.2 pct after grain boundary engineering. Kumar *et al.*<sup>[21]</sup> has suggested that the  $J_3$  junctions should be

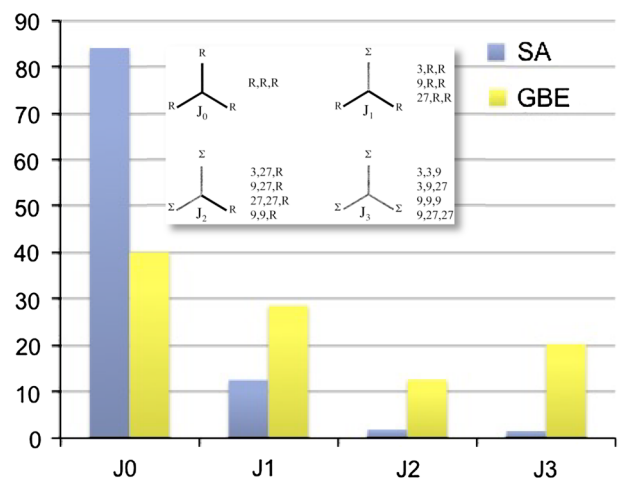


Fig. 3—Triple junction distributions of SA and grain boundary-engineered Inconel740H. The classification of triple junctions was inserted in the figure.

taken out of consideration because of their inactiveness in the process of arresting cracks along grain boundaries since the crack front is assumed never to reach them. A new parameter of resistant triple junction fraction was therefore defined as  $f_{J_2}/(1 - f_{J_3})$  to evaluate the effectiveness of triple junctions in arresting crack propagation. Here,  $f_{J_2}$  refers to the fraction of  $J_2$  junctions, which are able to arrest cracks, and  $1 - f_{J_3}$  is the

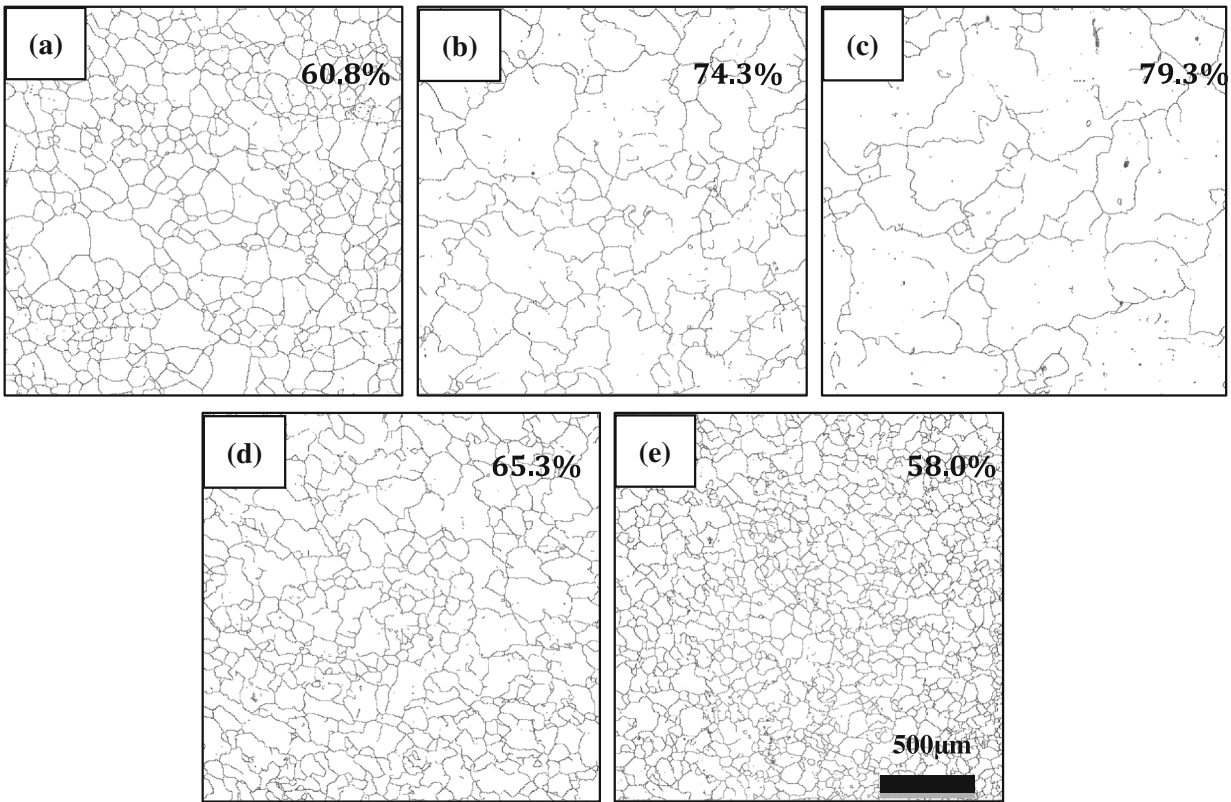


Fig. 4—The evolution of HAGB network with applied cold deformation (a) SA, (b) 3 pct, (c) 6 pct, (d) 10 pct, and (e) 15 pct.

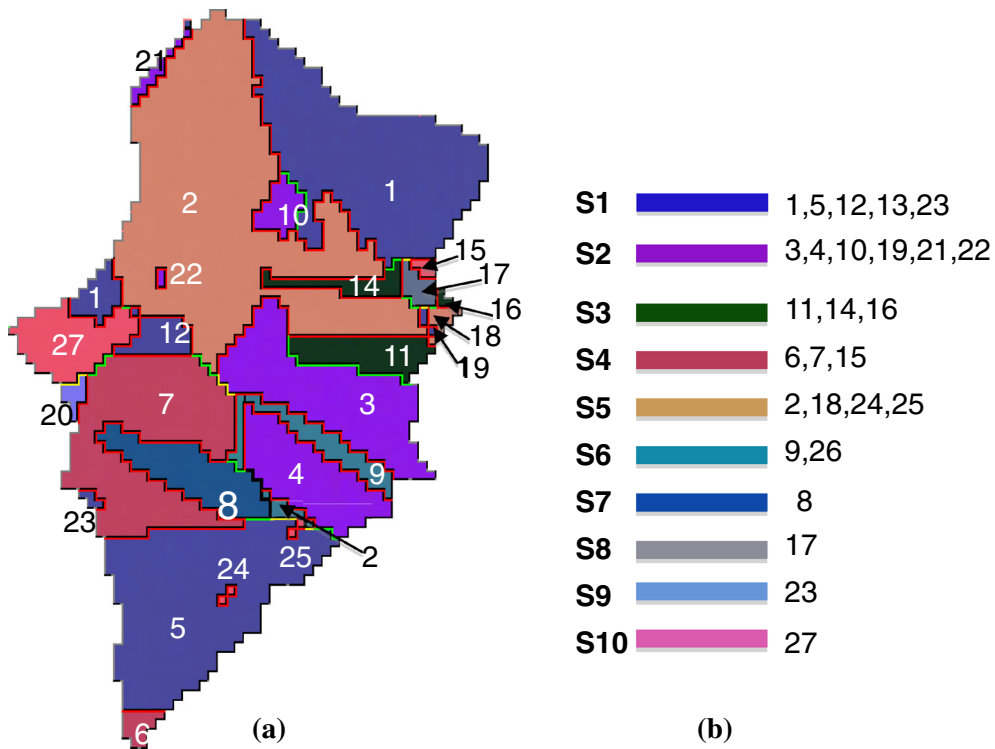


Fig. 5—Cluster analysis in grain boundary-engineered sample [6 pct cold deformation, 10 min annealing at 1373 K (1100 °C)] (a) grain cluster containing 27 grains; (b) the 27 grains inside the cluster were categorized into ten orientations.

**Table IV. Orientation Relationships of Each Grain Pair Inside the Cluster**

Orientations	S1	S2	S3	S4	S5	S6	S7	S8	S9
S2	39.7°[−101] Σ9/0.3°								
S3	38.8°[011] Σ9/0.7°	39.1°[−10−1] Σ9/0.9°							
S4	59.2°[1−1−1] Σ3/0.8°	32.0°[21 20 0] Σ27a/0.9°	59.2°[11−1] Σ3/0.8°						
S5	59.7°[11−1] Σ3/0.3°	59.9°[−111] Σ3/0.1°	59.8°[1−11] Σ3/0.2°	38.2°[101] Σ9/0.8°					
S6	59.2°[111] Σ3/0.8°	59.2°[1−11] Σ3/0.8°	35.5°[102] Σ27b/1.2°	59.2°[11−1] Σ3/0.8°	59.2°[1−11] Σ3/0.8°				
S7	38.4°[−101] Σ9/1.2°	59.9°[−111] Σ3/0.1°	59.2°[1−11] Σ3/0.8°	60.0°[−111] Σ3/0.1°	38.4°[−101] Σ9/1.3°	38.8°[101] Σ9/1.2°			
S8	31.5°[21 20 0] Σ27a/0.4°	39.1°[−10−1] Σ9/0.9°	59.5°[1−11] Σ3/0.5°	59.5°[11−1] Σ3/0.5°	38.5°[101] Σ9/1.1°	32.0°[21 20 0] Σ27a/0.8°	38.8°[101] Σ9/0.7°		
S9	38.8°[101] Σ9/1.1°	32.0°[21 20 0] Σ27a/0.9°	35.8°[01−2] Σ27b/1.1°	59.8°[111] Σ3/0.2°	38.4°[−101] Σ9/0.7°	59.2°[1−11] Σ3/0.8°	31.5°[21 20 0] Σ27a/1.2°	38.8°[101] Σ9/0.4°	
S10	59.6°[1−1−1] Σ3/0.4°	59.2°[1−11] Σ3/0.8°	35.1°[−10−2] Σ27b/1.1°	39.4°[−101] Σ9/0.6°	39.3°[0−1−1] Σ9/0.5°	38.4°[−101] Σ9/0.8°	59.7°[111] Σ3/0.3°	31.5°[21 20 0] Σ27a/0.9°	38.8°[1−1 0] Σ9/0.9°

fraction of triple junctions except  $J3$  junctions, thereby representing the frequency of triple junctions that are active in arresting cracks. As shown in Figure 3, there are substantial increase in the fractions of both  $J2$  and  $J3$  junctions for the grain boundary-engineered sample. Therefore, the resistant triple junction fraction is expected to increase significantly after grain boundary engineering.

### 2. Cluster analysis

The microstructures of SA and thermo-mechanically treated samples by annealing at 1373 K (1100 °C) for 20 minutes after compressed to different strains (3, 6, 10, and 15 pct) are shown in Figure 4. Only HAGBs are shown to delineate the HAGB network. The corresponding  $f_{cs1}$  values are also given in the figures. It is found that  $f_{cs1}$  agrees well with the level of HAGB network discontinuity. Samples annealed after 3.3 and 6.7 pct strains exhibited the highest values of  $f_{cs1}$  and levels of HAGB network discontinuity, while for samples annealed after 10 pct compression,  $f_{cs1}$  drops to nearly the same value as that of the SA sample. In addition, the HAGB network is as well connected as that of the SA sample.

A cluster defines an area bounded by HAGBs and cluster analysis is commonly used in grain boundary engineering investigations.<sup>[21,24,26]</sup> An example of a cluster in a grain boundary-engineered sample is shown in Figure 5. This cluster contains 27 grains, which are numbered in the figure. By considering the EBSD data, these 27 grains can be categorized into ten different orientations, as listed in Figure 5(b). The misorientations between any two of these orientations together with the nearest misorientation are listed in Table IV. It is found that any pair of orientations inside the cluster is related by a  $\Sigma 3^n$  misorientation.

The average grain size (including twin boundaries) and cluster size (ignoring twin boundaries) for different applied strains were measured using a linear intercept method in Channel 5 software are shown in Figure 6. At

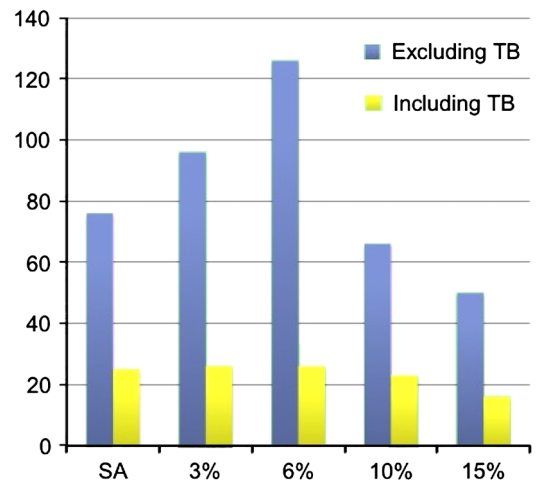


Fig. 6—The evolution of grain size (including twin boundaries) and cluster size (excluding twin boundaries) with applied cold deformation.

least 500 grains or clusters from ten different areas were measured for each sample to exclude the diversity in grain size. It is found that the cluster sizes of samples compressed by 3 and 6 pct are much larger than that in SA sample. It is supposed that the stored strain energy after small amounts of strain (3 and 6 pct) is not sufficient enough to induce recrystallization. Instead, two modifications in the microstructure might occur during annealing after applying such small amounts of strain. First, the dislocation density generated by deformation might be enough to cause the formation of incoherent twin boundaries with high mobility, which then migrate and interact with twin boundaries inside the grains.<sup>[28]</sup> Thereby large amounts of  $\Sigma 3$ – $\Sigma 3$ – $\Sigma 9$ ,  $\Sigma 3$ – $\Sigma 9$ – $\Sigma 27$  triple junctions can be introduced into the HAGB network. As a result, the fraction of CSL boundaries and the cluster size is raised, and the connectivity of HAGB network is significantly interrupted. Second, during deformation extrinsic grain



boundary dislocations (EGBDs) might be generated, which may be annihilated during subsequent annealing by climb.<sup>[8]</sup> It is reported by Pumphrey and Gleiter<sup>[29]</sup> that during annealing the thermal driving force together with the strain field associated with EGBDs may cause the migration of grain boundaries. During grain boundary migration, multi-twinning process takes place, leading to an increase in both the CSL boundary fraction and cluster size. In samples annealed after 10 and 15 pct strains, the cluster sizes are found to be nearly the same as that in the initial SA sample, with a well-connected HAGB network. Moreover, many small equiaxed grains are observed between the large grains, indicating the occurrence of recrystallization. The cluster size for the 15 pct strain sample was smaller compared to that of the 10 pct strain sample, suggesting more nucleation sites during recrystallization in the larger strain sample. Newly formed HAGBs migrate easily during recrystallization and interact with lattice dislocations and  $\Sigma 3$  boundaries inside the grains. When

HAGBs interact with lattice dislocations, new coherent twin boundaries can form inside the grains and these do not contribute to the interruption of the HAGB network. The interaction between HAGBs and  $\Sigma 3$  boundaries inside grains will produce another HAGB rather than a  $\Sigma 3$  boundary.<sup>[29]</sup> As a result, the fractions of  $\Sigma 3$  boundaries and total CSL boundaries remain unchanged. The connectivity of HAGBs is not broken up.

It is generally known that grain growth is always accompanied with high temperature annealing, *i.e.*, 1373 K (1100 °C) in this study, which might cause doubt in the effect of applied strain on the significant increase in cluster size. Therefore, the grain boundary microstructure of the sample annealed at 1373 K (1100 °C) for 20 minutes without strain is compared with that of SA sample as well as strain-annealed sample in Figure 7. It is found that the grain growth during the 1373 K (1100 °C)/20 minutes annealing is marginal. In comparison, the cluster size of strain-annealed sample is much larger than that of the annealed sample. The

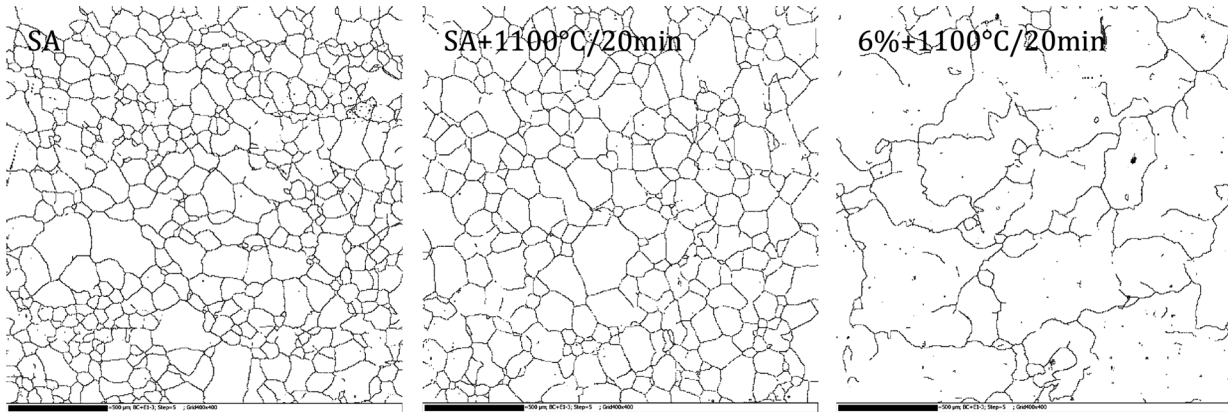


Fig. 7—The grain boundary microstructures showing only HAGBs of samples of SA, annealed, and strain annealed.

Table V. Thermal Stability of the GBCD for the Grain Boundary-Engineered Sample

Length Fraction/pct	Total $\Sigma$	$\Sigma 3$	$\Sigma 9$	$\Sigma 27$
6 pct + 1373 K (1100 °C)/20 min	79.3	69.2	6.32	3.75
6 pct + 1373 K (1100 °C)/20 min + 1023 K (750 °C)/500 h	78.6	67.8	6.53	4.26

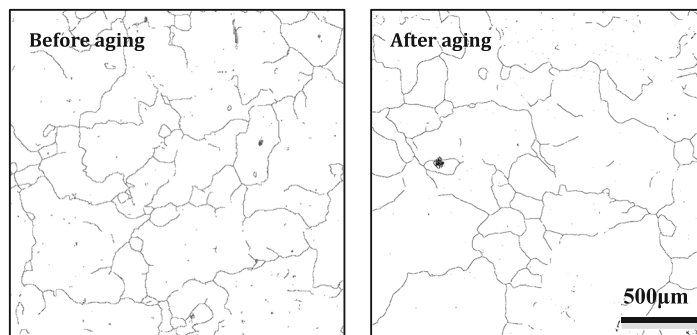


Fig. 8—The GBCD of grain boundary-engineered samples before and after aging at 1023 K (750 °C) for 500 h.

HAGB network is well connected in the annealed sample while significantly interrupted in the strain-annealed sample. This comparison clarified the doubt of the contribution of applied strains on the cluster size increase during subsequent annealing. In addition, the ratios of  $\Sigma 3$  to HAGB in SA, annealed, and strain-annealed samples are calculated to be 1.51, 1.59, and 3.30, respectively. The ratio in strain-annealed sample is twice than that in annealed sample, further confirming the occurrence of multi-twinning during grain boundary engineering.

#### D. The Thermal Stability of GBE-Optimized Microstructure

The alloy will be used at 1023 K (750 °C) for a long period of time. Thus, it is necessary to evaluate also the thermal stability of the optimized GBCD microstructure. For this, a sample annealed at 1373 K (1100 °C) for 20 minutes after an applied strain of 6 pct was aged at 1023 K (750 °C) for 500 hours and then cooled in air. The CSL boundary fractions before and after aging are shown in Table V. No evident change in the fractions of each CSL boundary type was found. In addition, the HAGB networks of the samples before and after aging are shown in Figure 8. It is found that the highly interrupted HAGB network and large cluster size before after grain boundary engineering are preserved after aging, therefore confirming the thermal stability of the optimized Inconel740H microstructure during service

### IV. CONCLUSIONS

A grain boundary engineering investigation of the Ni-base superalloy Inconel740H was conducted using single-step thermomechanical processing treatments. Four different strains (3, 6, 10, and 15 pct) and four different annealing durations (5, 10, 20, 40 minutes) at 1373 K (1100 °C) were investigated. The following conclusions can be drawn from the results.

- (1) For samples annealed after strains of 3 and 6 pct,  $f_{\text{CSL}}$  increases with annealing time until 20 minutes with no further increase for longer durations. The highest value of  $f_{\text{CSL}}$  (around 80 pct, compared with 60 pct in the solution-annealed sample) was obtained in a sample deformed by 6 pct followed by annealing at 1373 K (1100 °C) for 20 minutes. For samples annealed after deformation to strains of 10 and 15 pct, there is no significant increase in  $f_{\text{CSL}}$  is seen for any annealing time.
- (2) The fractions of  $J_2$  and  $J_3$  type junctions (triple junctions containing 2 or 3 CSL boundaries, respectively) increased after grain boundary engineering. Therefore, the resistant triple junction fraction, defined as  $f_{J_2}/(1 - f_{J_3})$ , increases substantially after grain boundary engineering, which is believed to be beneficial in arresting crack propagation.
- (3) Cluster analysis of the grain boundary-engineered samples indicates that the size of the cluster correlates well with CSL boundary fractions, as well as HAGB

network connectivity. Only several clusters with size larger than 500  $\mu\text{m}$  exist in the microstructure of the sample processed under optimal conditions.

- (4) Long-time annealing of a sample processed to give an optimal microstructure shows that the microstructure is stable at 1023 K (750 °C) such that the interrupted HAGB network is retained. Nevertheless, longer aging time is required so as to further confirm the microstructure stability after grain boundary engineering, which would be the subject of future work.

### ACKNOWLEDGMENTS

The authors are grateful to the financial support from the High-Tech Research and Development Project (No. 2102AA03A501) supported by National Ministry of Science and Technology of China.

### REFERENCES

1. S. Zhao, X. Xie, G.D. Smith, and S.J. Patel: *Mater. Lett.*, 2004, vol. 58, pp. 1784–87.
2. S. Zhao, X. Xie, G.D. Smith, and S.J. Patel: *Mater. Sci. Eng.*, 2002, vol. 355A, pp. 96–105.
3. S. Zhao, X. Xie, G.D. Smith, and S.J. Patel: *Mater. Des.*, 2006, vol. 27, pp. 1120–27.
4. Y. Chong, Z.D. Liu, A. Godfrey, W. Liu, and Y.Q. Weng: *Mater. Sci. Eng.*, 2014, vol. 589A, pp. 153–64.
5. Y. Chong, Z.D. Liu, A. Godfrey, W. Liu, and Y.Q. Weng: *Philos. Mag. Lett.*, 2013, vol. 93, pp. 688–96.
6. J.P. Shingledecker and G.M. Pharr: *Metall. Mater. Trans. A*, 2012, vol. 43A, pp. 1902–10.
7. T. Watanabe: *Res. Mech.*, 1984, vol. 11, pp. 47–84.
8. V. Randle: *Philos. Mag. A*, 1993, vol. 67, pp. 1301–16.
9. V. Thaveerungsriporn and G.S. Was: *Metall. Mater. Trans. A*, 1997, vol. 21A, pp. 2101–12.
10. U. Krupp, W.M. Kane, X. Liu, O. Dueber, C. Laird, and C.J. McMahon: *Mater. Sci. Eng.*, 2003, vol. A349, pp. 213–25.
11. B. Alexandreanu, B. Capell, and G.S. Was: *Mater. Sci. Eng.*, 2001, vol. A300, pp. 94–104.
12. M. Shimada, H. Kokawa, Z.J. Wang, Y.S. Sato, and I. Karibe: *Acta Mater.*, 2002, vol. 50, pp. 2331–41.
13. D.C. Crawford and G.S. Was: *Metall. Trans.*, 1992, vol. 23A, pp. 1195–206.
14. E.A. West and G.S. Was: *J. Nucl. Mater.*, 2009, vol. 392, pp. 264–71.
15. C.J. Boehlert, S.C. Longanbach, and T.R. Bieler: *Philos. Mag.*, 2008, vol. A88, pp. 641–64.
16. C.J. Boehlert, D.S. Dickmann, and N.C. Eisinger: *Metall. Mater. Trans. A*, 2006, vol. 37A, pp. 27–40.
17. T. Watanabe and S. Tsurekawa: *Acta Mater.*, 1999, vol. 47, pp. 4171–85.
18. M.L. Kronberg and F.H. Wilson: *Trans. AIME*, 1949, vol. 185, pp. 501–17.
19. H. Grimmer, W. Bollmann, and D.H. Warrington: *Acta Crystallog.*, 1974, vol. A30, pp. 197–205.
20. V. Randle: *Acta Mater.*, 2004, vol. 52, pp. 4067–81.
21. M. Kumar, W.E. King, and A.J. Schwartz: *Acta Mater.*, 2000, vol. 48, pp. 2081–91.
22. V.Y. Gertsman and K. Tangri: *Acta Metall. Mater.*, 1995, vol. 43, pp. 2317–24.
23. S. Tsurekawa, S. Nakamichi, and T. Watanabe: *Acta Mater.*, 2006, vol. 54, pp. 3617–26.
24. C.A. Schuh, M. Kumar, and W.E. King: *Acta Mater.*, 2003, vol. 51, pp. 686–700.
25. L. Tan, K. Sridharan, and T.R. Allen: *J. Nucl. Mater.*, 2003, vol. 371, pp. 171–75.



26. S. Xia, B.X. Zhou, W.J. Chen, and W.G. Wang: *Scripta Mater.*, 2006, vol. 54, pp. 2019–22.
27. L. Tan and T.R. Allen: *Metall. Mater. Trans. A*, 2005, vol. 36A, pp. 1921–25.
28. X.Y. Fang, K. Zhang, H. Guo, W.G. Wang, and B.X. Zhou: *Mater. Sci. Eng.*, 2008, vol. A487, pp. 7–13.
29. P. Pumphrey and H. Gleiter: *Philos. Mag.*, 1971, vol. 35, pp. 365–70.